Supporting Information for

Surface defect strategy of NiCo-layered double hydroxide decorated MXene layers for durable solid-state supercapacitors

Jinhe Wei [a,b], Fei Hu [a,b], Chenglong Lv [a,b], Limin Bian [a,b], He Liu [a,b], Qiuyun Ouyang [a,b,*]

[a] Key Laboratory of Photonic Materials and Devices Physics for Oceanic Applications, Ministry of Industry and Information Technology of China, College of Physics and Optoelectronic Engineering, Harbin Engineering University, Harbin 150001, China

[b] Key Laboratory of In-Fiber Integrated Optics of Ministry of Education, College of Physics and Optoelectronic Engineering, Harbin Engineering University, Harbin 150001, China

[*] *Corresponding author:* qyouyang@hrbeu.edu.cn

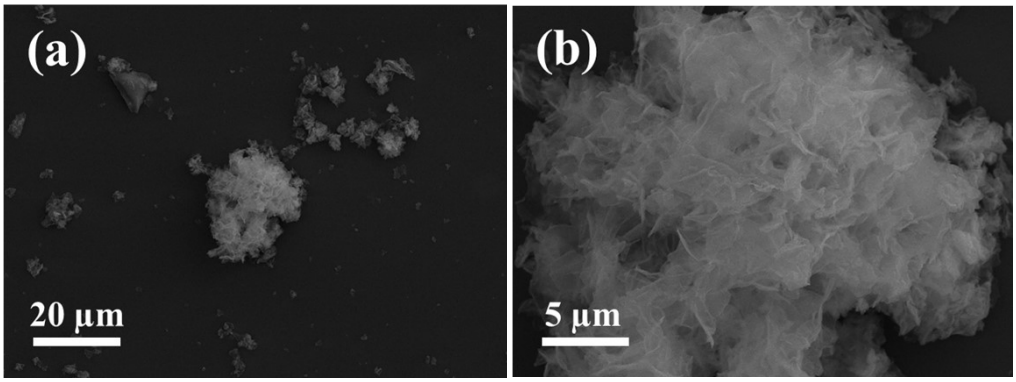

Fig. S1 SEM images of (a,b) NiCo-LDH at different magnification.

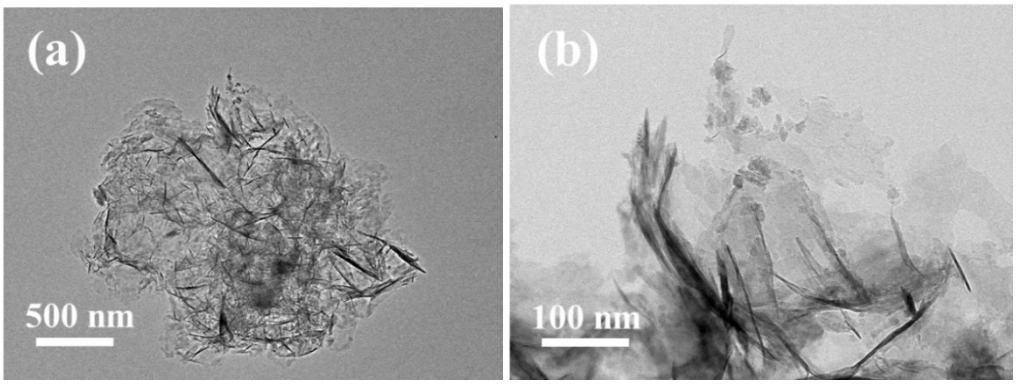

Fig. S2 TEM images of (a,b) NiCo-LDH at different magnification.

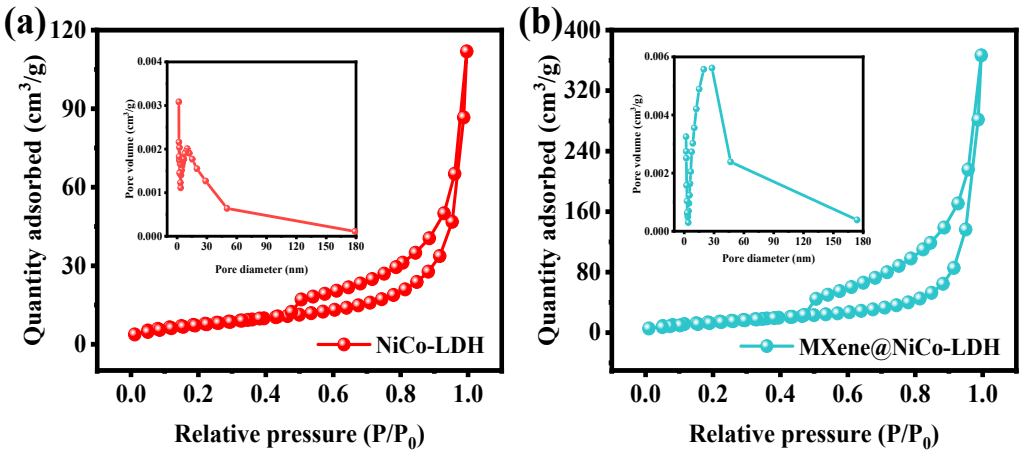

Fig. S3 The BET isotherm and pore size distribution profile of (a) NiCo-LDH and (b) MXene@NiCo-LDH.

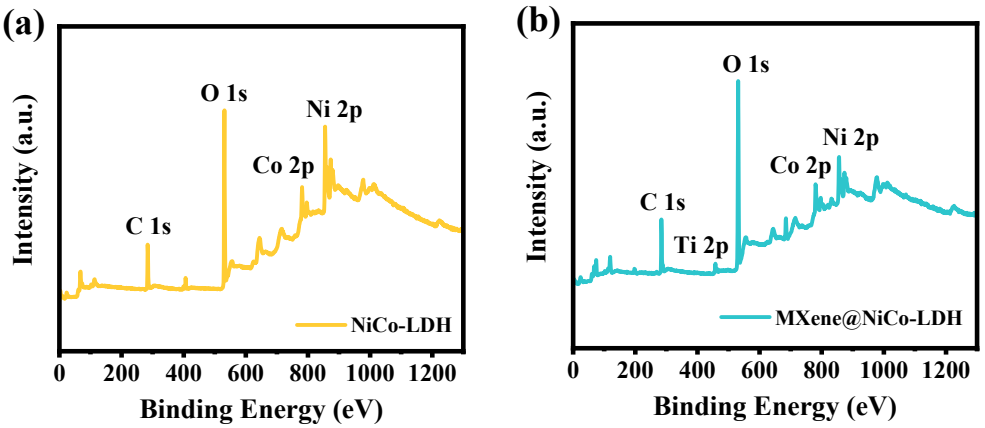

Fig. S4 The XPS spectra of (a) NiCo-LDH and (b) MXene@NiCo-LDH samples: Survey spectrum.

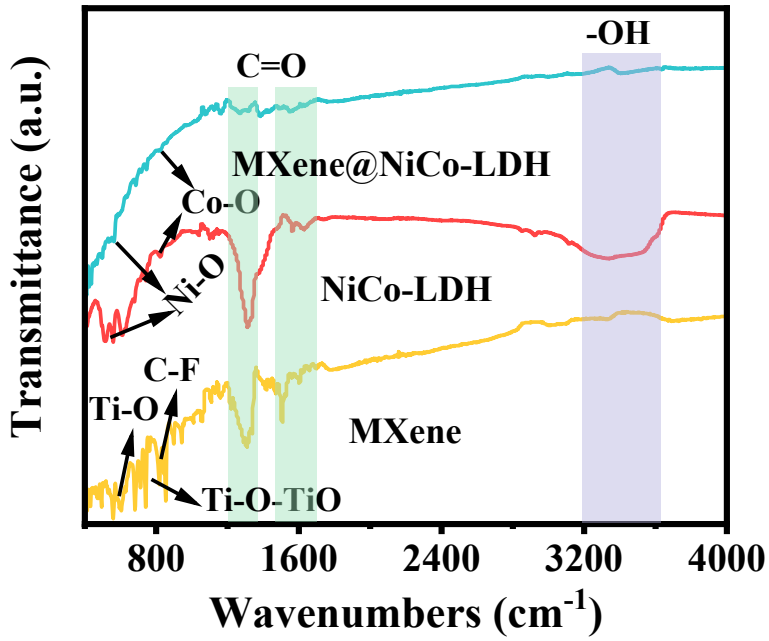

Fig. S5 FT-IR spectra of MXene, NiCo-LDH and MXene@NiCo-LDH.

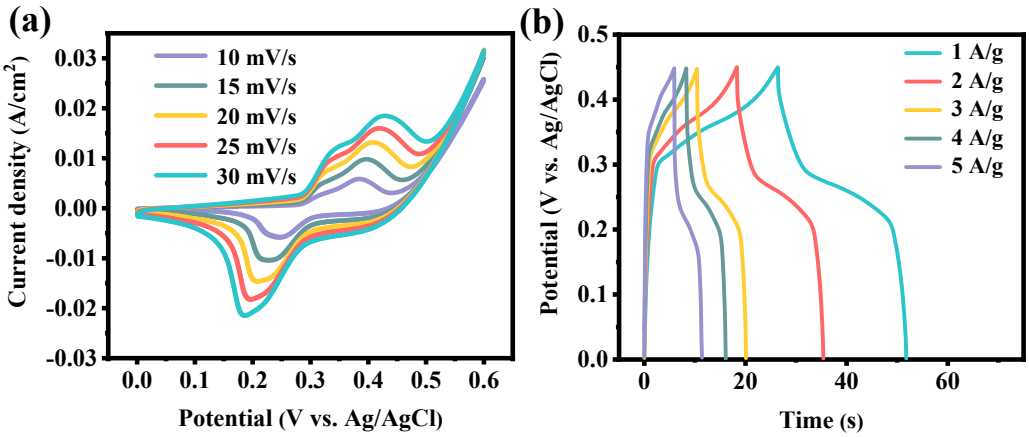

Fig. S6 (a) CV curves of NF electrode at different scan rates; (b) GCD curves of NF electrode at different specific currents.

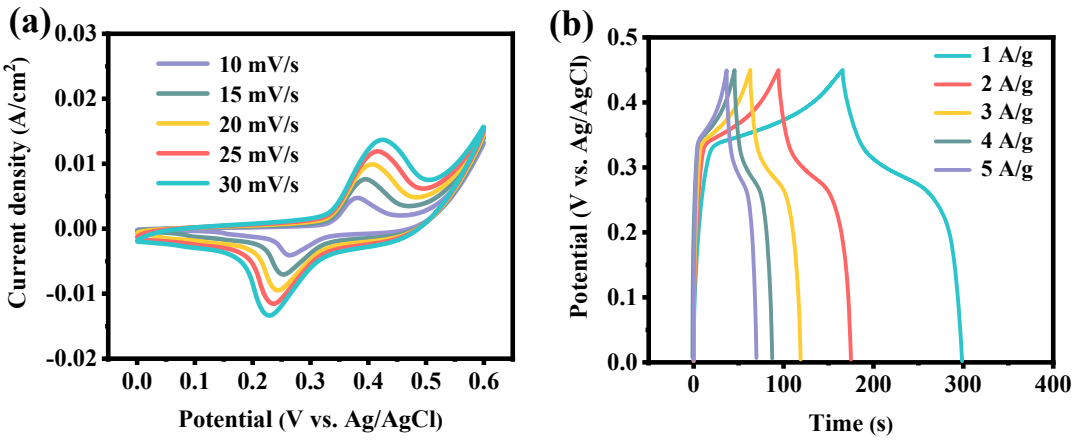

Fig. S7 (a) CV curves of MXene electrode at different scan rates; (b) GCD curves of MXene electrode at different specific currents.

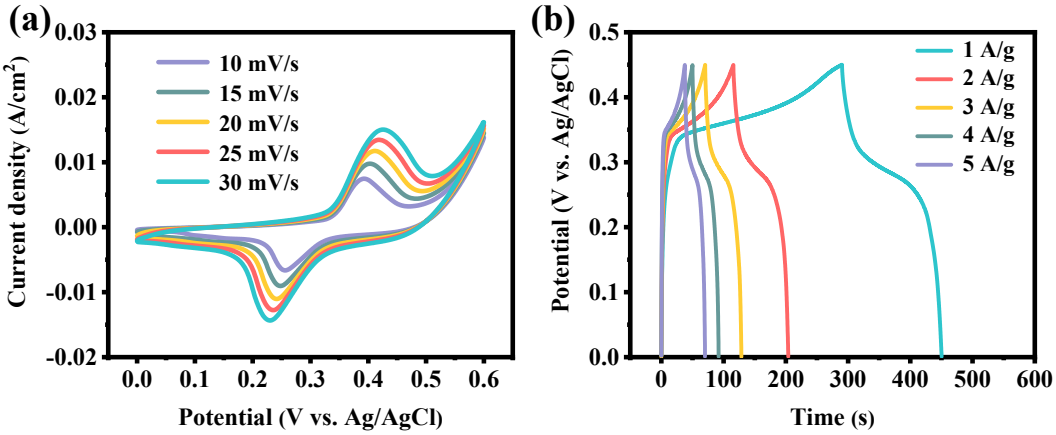

Fig. S8 (a) CV curves of NiCo-LDH electrode at different scan rates; (b) GCD curves of NiCo-LDH electrode at different specific currents.

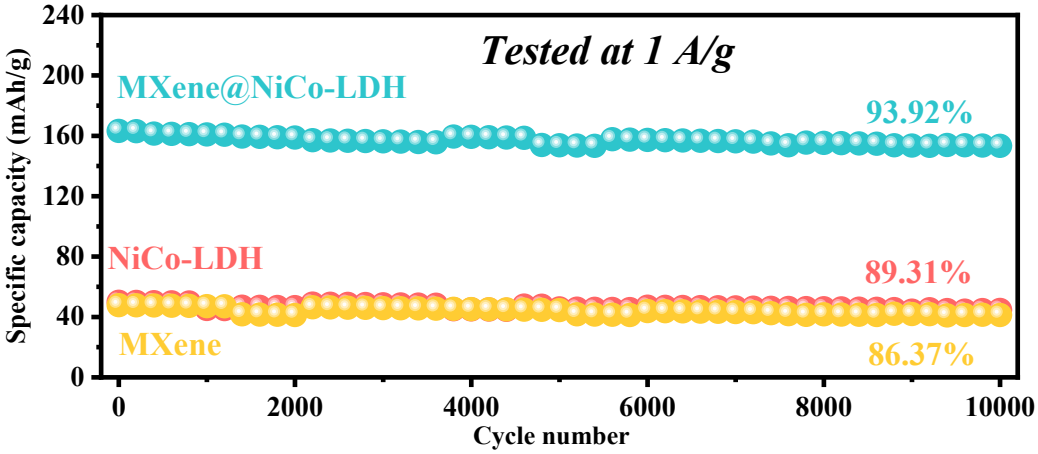

Fig. S9 Cycling stability for 10000 cycles of as-prepared electrode.

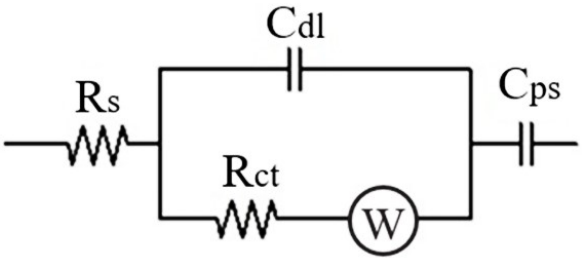

Fig. S10 Circuit used to fit EIS data.

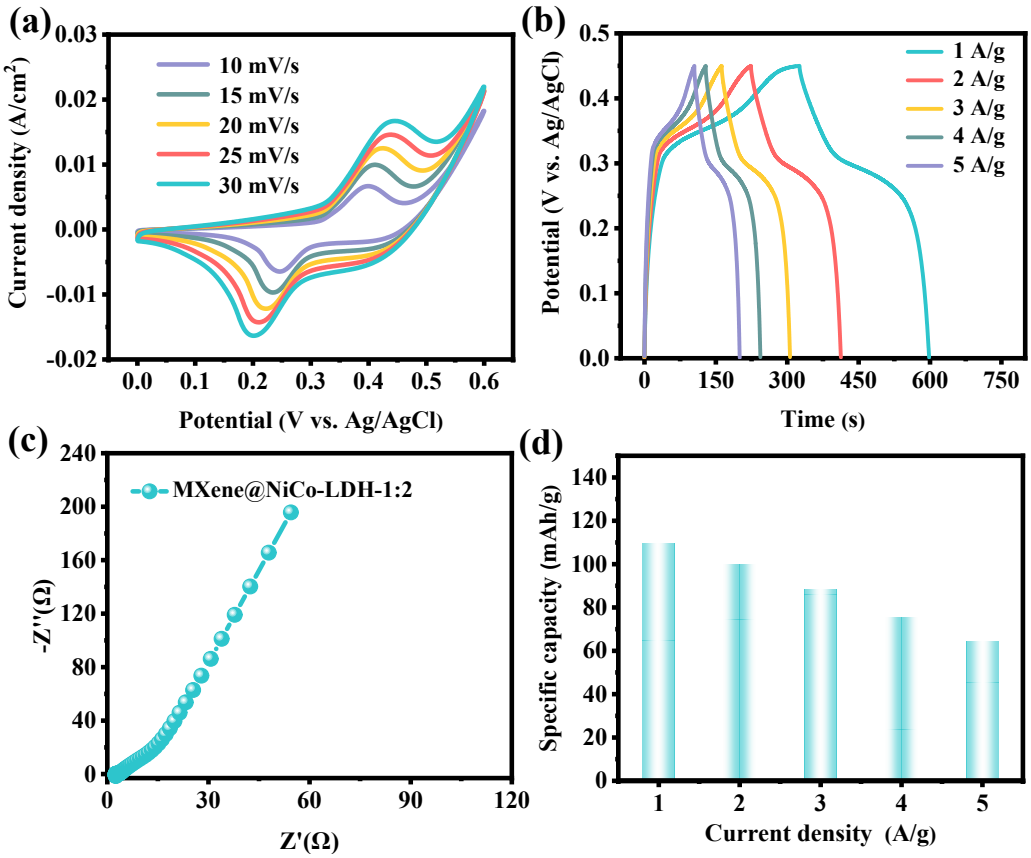

Fig. S11 (a) CV curves of MXene@NiCo-LDH-1:2 electrode at different scan rates; (b) GCD curves of MXene@NiCo-LDH-1:2 electrode at different specific currents; (c) EIS curves; (d) Specific capacitance of MXene@NiCo-LDH-1:2 electrode.

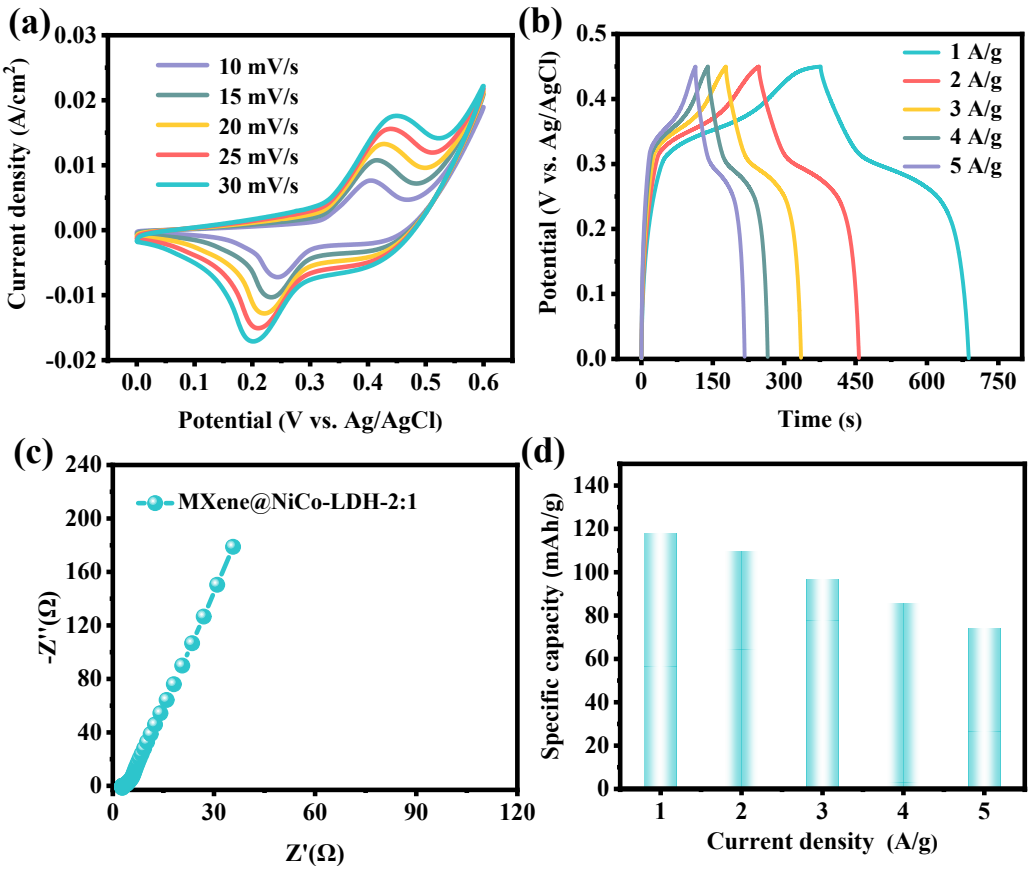

Fig. S12 (a) CV curves of MXene@NiCo-LDH-2:1 electrode at different scan rates; (b) GCD curves of MXene@NiCo-LDH-2:1 electrode at different specific currents; (c) EIS curves; (d) Specific capacitance of MXene@NiCo-LDH-2:1 electrode.

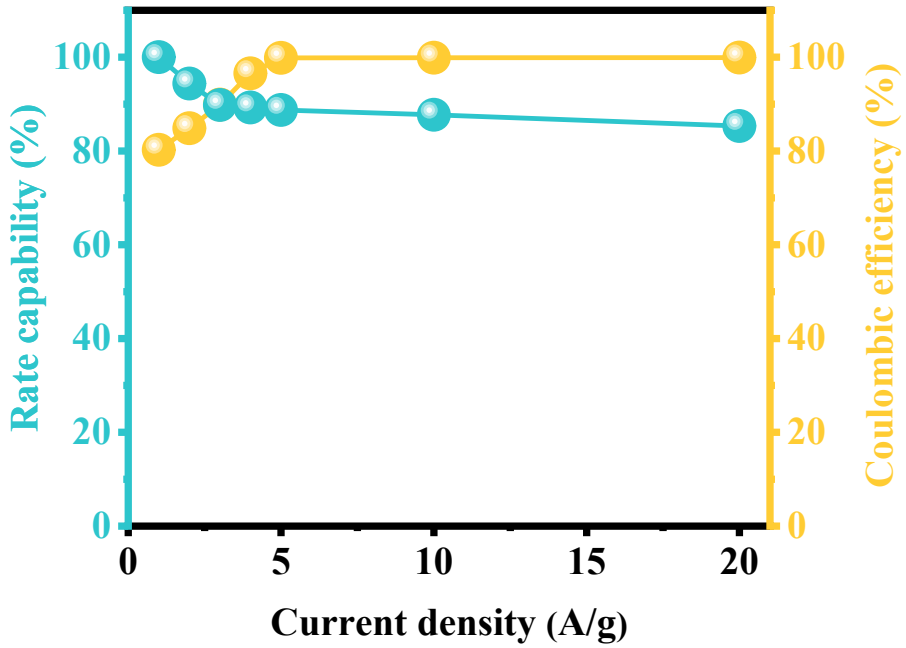

Fig. S13 Rate capability and coulombic efficiency of the MXene@NiCo-LDH.

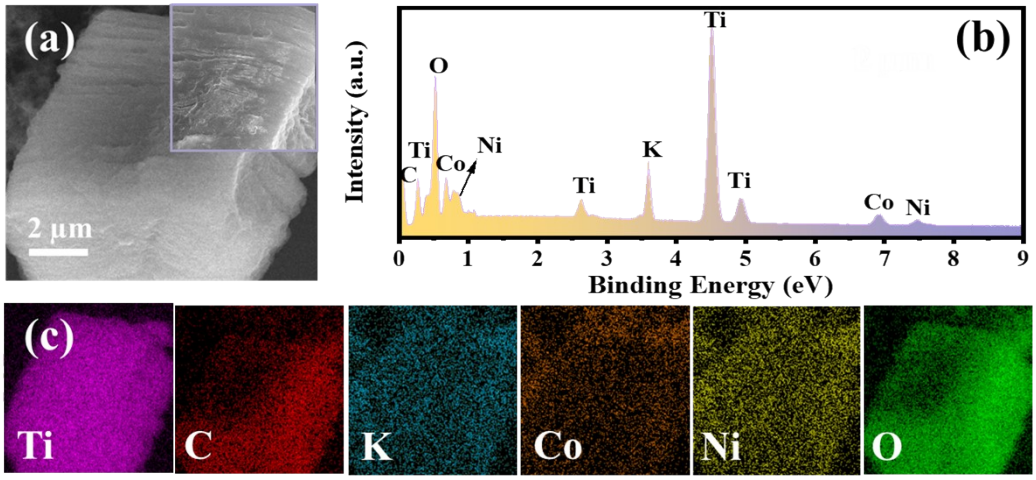

Fig. S14 Post-electrochemical characterization of MXene@NiCo-LDH after stability test (a) SEM image; (b) SEM-EDX spectrum; (c) Elemental mapping area and elemental mapping spectra of different elements.

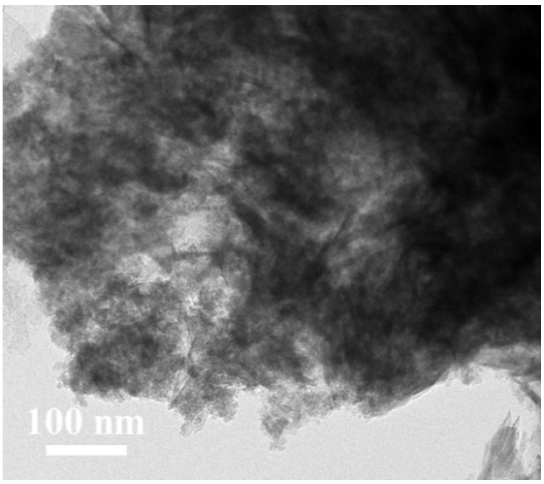

Fig. S15 TEM images of MXene@NiCo-LDH after electrochemical test.

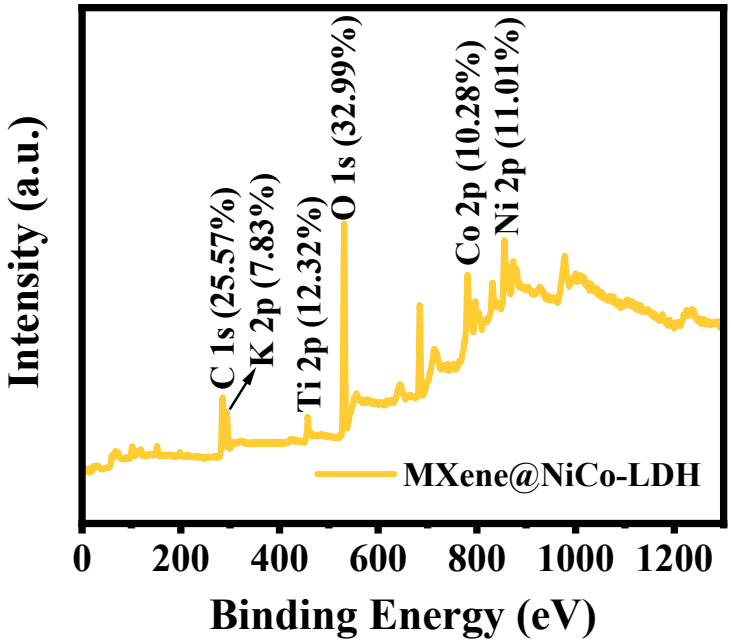

Fig. S16 XPS survey spectra of MXene@NiCo-LDH after the electrochemical test.

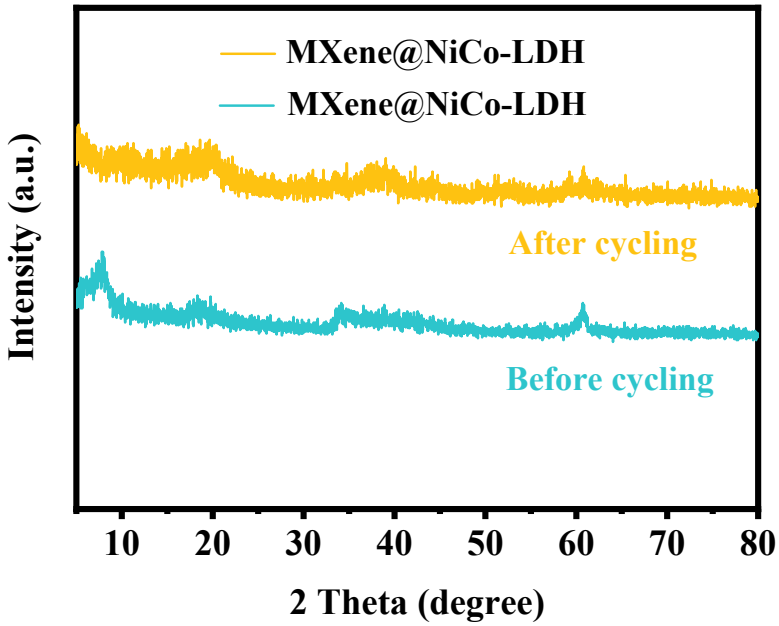

Fig. S17 XRD patterns of MXene@NiCo-LDH before and after electrochemical stability test.

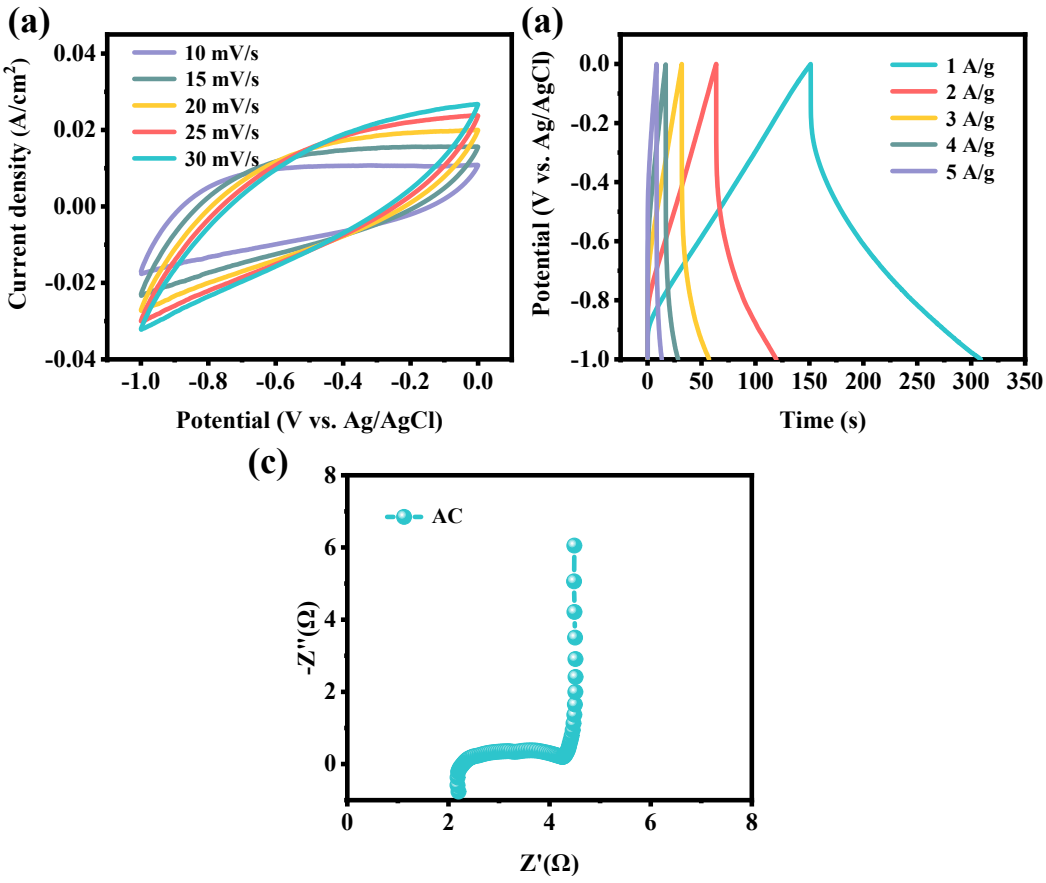

Fig. S18 (a) CV curves of AC; (b) GCD curves of AC; (c) EIS curve of AC.

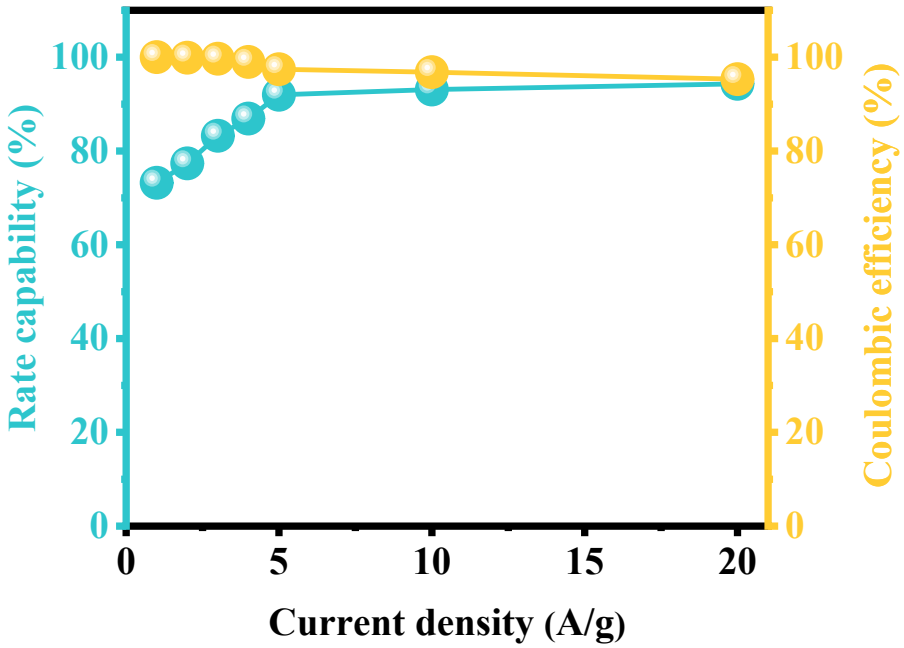

Fig. S19 Rate capability and coulombic efficiency of the MXene@NiCo-LDH//AC.

Table S1 Calculation of adsorption energy of hydroxyl group on MXene@NiCo-LDH.

DFT calculation				
Materials	**Slab**	**Slab+OH^-**	**OH^-**	**Adsorption energy**
NiCo-LDH	-1847.63	-1856.09	-6.12	-2.34
MXene@NiCo-LDH	-3292.58	-3302.17	-6.12	-3.47

Table S2 The electrochemical properties of the MXene based nanocomposite supercapacitors.

Electrode materials	Electrolyte	Potential window [V]	Performance	Cyclic stability	Ref.
MXene@NiCo-LDH	**2 M KOH**	**0 to 0.45**	**1306 F·g^{-1} at 1 A·g^{-1} (163.25 mAh·g^{-1} at 1 A·g^{-1})**	**93.92 % after 10000 cycles**	**This work**
MoS_2/MXene	3 M KOH	-0.8 to 0	583 F·g^{-1} at 1 A·g^{-1}	96.5 % after 5000 cycles	[1]
CoF/MXene	1 M KOH	0 to 0.4	1268.7 F·g^{-1} at 1 A·g^{-1}	96 % after 5000 cycles	[2]
PPy/MXene@CF	1 M H_2SO_4	0 to 0.5	506.6 F·g^{-1} at 1 A·g^{-1}	83.3 % after 2000 cycles	[3]
MnO_2@MXene/CNT	1 M Na_2SO_4	0 to 1.0	181.8 F·g^{-1} at 1 A·g^{-1}	91 % after 5000 cycles	[4]
MXene@MnO_2	1 M Na_2SO_4	0 to 1.0	348.5 F·g^{-1} at 0.5 A·g^{-1}	91.9 % after 5000 cycles	[5]
MXene@CNT-KOH	3 M H_2SO_4	-0.6 to 0.2	404.4 F·g^{-1} at 1 A·g^{-1}	99 % after 20000 cycles	[6]
MXene@CNTs	1 M H_2SO_4	0.2 to -0.8	300 F·g^{-1} at 1 A·g^{-1}	92 % after 10000 cycles	[7]
$CoSe_2$/Ni_3Se_4/MXene	3 M KOH	0 to 0.5	283 mAh·g^{-1} at 1 A·g^{-1}	80 % after 5000 cycles	[8]
$NiCo_2S_4$@$Ti_3C_2T_x$	3 M KOH	0 to 0.55	1076 F·g^{-1} at 1 A·g^{-1}	80 % after 5000 cycles	[9]
$NiCo_2S_4$/$Ti_3C_2T_x$	0.5 M K_2SO_4	-0.2 to 0.5	167.28 F·g^{-1} at 4 A·g^{-1}	81 % after 3000 cycles	[10]
$Ti_3C_2T_x$@NiO-RGO	1 M KOH	0 to 1	966 F·g^{-1} at 1 A·g^{-1}	94.5 % after 10000 cycles	[11]

Table S3 The electrochemical properties of the NiCo-LDH based nanocomposite supercapacitors.

Electrode materials	Electrolyte	Potential window [V]	Performance	Cyclic stability	Ref.
MXene@NiCo-LDH	2 M KOH	0 to 0.45	1306 $F \cdot g^{-1}$ at 1 $A \cdot g^{-1}$ (163.25 $mAh \cdot g^{-1}$ at 1 $A \cdot g^{-1}$)	93.92 % after 10000 cycles	This work
Ni_2Co_1-LDHs/BC50	6 M KOH (34–35°)	-0.1 to 0.30	2390 $F \cdot g^{-1}$ at 1 $A \cdot g^{-1}$	75.9 % after 4000 cycles	[12]
Ni_xCo_{1-x} LDH/AC	6 M KOH	0 to 0.45	947 $F \cdot g^{-1}$ at 1 $A \cdot g^{-1}$	83.5 % after 5000 cycles	[13]
NiAl/LDH	6 M KOH	0 to 0.55	884.5 $F \cdot g^{-1}$ at 1 $A \cdot g^{-1}$	90 % after 7000 cycles	[14]
Ni@Co-Fe/LDH	6 M KOH	-0.8 to 0	1289 $F \cdot g^{-1}$ at 1 $A \cdot g^{-1}$	76.66 % after 5000 cycles	[15]
$Co(OH)_2$@NiCo/LDH	2 M KOH	0 to 0.5	996 $F \cdot g^{-1}$ at 1 $A \cdot g^{-1}$	75.46 % after 5000 cycles	[16]
Ni_2CoMn_1/LDH	3 M KOH	0 to 0.5	1634.4 $F \cdot g^{-1}$ at 0.5 $A \cdot g^{-1}$	73.1 % after 2000 cycles	[17]
NiMn-LDH	3 M KOH	0 to 0.45	1010.4 $F \cdot g^{-1}$ at 0.2 $A \cdot g^{-1}$	70 % after 5000 cycles	[18]
Co-Al LDH/graphene	6 M KOH	0 to 0.55	712 $F \cdot g^{-1}$ at 1 $A \cdot g^{-1}$	81 % after 2000 cycles	[19]
NiCo-LDH/NCF	2 M KOH	0 to 0.5	756 $C \cdot g^{-1}$ at 0.5 $A \cdot g^{-1}$	54.7% from 0.5 to 20 $A \cdot g^{-1}$	[20]
NiCoMn LDH/rGO	2 M KOH	0 to 0.5	912 $F \cdot g^{-1}$ at 1 $A \cdot g^{-1}$	63.3 % after 2500 cycles	[21]

Table S4 Comparison of the electrochemical performances of MXene@NiCo-LDH composites with similar electrode materials.

Electrode materials	Electrolyte	Potential window [V]	Performance	Cyclic stability	Ref.
MXene@NiCo-LDH	**2 M KOH**	**0 to 0.45**	**1306 F·g^{-1} at 1 A·g^{-1} (163.25 mAh·g^{-1} at 1 A·g^{-1})**	**93.92 % after 10000 cycles**	**This work**
QD-$Ti_3C_2Cl_2$@ NiAlLDHs	1 M KOH	0 to 0.6	2010.8 F·g^{-1} at 1 A·g^{-1}	94.1 % after 10000 cycles	[22]
MXene/NiCo-LDHs	1 M $(NH_4)_2SO_4$	0 to 0.6	1207 F·g^{-1} at 0.5 A·g^{-1}	93 % after 5000 cycles	[23]
V_2CT_x/NiV-LDH	6 M KOH	0 to 0.5	1658.19 F·g^{-1} at 1 A·g^{-1}	80.95 % after 10000 cycles	[24]
Fe_1Ni_3-LDH/$Ti_3C_2T_x$-MXene	6 M KOH	0 to 0.45	1015 F·g^{-1} at 1 A·g^{-1}	88 % after 10000 cycles	[25]
$NiCo_2$-LDHs@MXene/rGO	2 M KOH	0 to 0.45	332.2 mAh·g^{-1} at 1 A·g^{-1}	87.5 % after 5000 cycles	[26]
Ni_2CoLDHs@AL-Ti_3C_2 MXene	6 M KOH	0 to 0.5	227 mAh·g^{-1} at 1 A·g^{-1}	90 % after 10000 cycles	[27]
Ti_3C_2/Ni-Co-Al-LDH	1 M KOH	0 to 0.6	748.2 F·g^{-1} at 1 A·g^{-1}	748.2 to 569.8 F·g^{-1} from 1 to 20 A·g^{-1}	[28]
LDH-MXene-LDH	6 M KOH	0 to 0.5	179 mAh·g^{-1} at 1 A·g^{-1}	79.1 % after 5000 cycles	[29]
NiMn-LDH/MXene	6 M KOH	0 to 0.45	1575 F·g^{-1} at 0.5 A·g^{-1}	90.3 % after 10000 cycles	[30]
NiMn-LDH/MXene	1 M $LiPF_6$	0 to 0.4	133 mAh·g^{-1} at 1 A·g^{-1}	88.6 % after 3000 cycles	[31]

Table S5 Nyquist impedance parameters of the different positrodes (MXene, NiCo-LDH, MXene@NiCo-LDH).

Sample	R_s [Ω]	R_{ct} [Ω]	R_w [Ω]
MXene	3.87	2.31	0.48
NiCo-LDH	3.61	1.33	0.54
MXene@NiCo-LDH	2.10	1.10	0.12

Table S6 Nyquist impedance parameters of MXene@NiCo-LDH//AC before and after stability.

Sample MXene@NiCo-LDH//AC	R_s [Ω]	R_{ct} [Ω]	R_w [Ω]
Before stability	4.14	1.39	0.43
After stability	4.51	1.72	0.67

References

1. B. Kirubasankar, M. Narayanasamy, J. Yang, M. Y. Han, W. H. Zhu, Y. J. Su, S. Angaiah and C. Yan, Construction of heterogeneous 2D layered MoS_2/MXene nanohybrid anode material via interstratification process and its synergetic effect for asymmetric supercapacitors, *Appl. Surf. Sci.*, 2020, **534**, 14764.
2. I. Ayman, A. Rasheed, S. Ajmal, A. Rehman, A. Ali, I. Shakir and M. F. Warsi, $CoFe_2O_4$ nanoparticle-decorated 2D MXene: a novel hybrid material for supercapacitor applications, *Energy Fuels*, 2020, **34**, 7622–7630.
3. L. J. Yang, F. Lin, F. Zabihi, S. Y. Yang and M. F. Zhu, High specific capacitance cotton fiber electrode enhanced with PPy and MXene by in situ hybrid polymerization, *Int. J. Biol. Macromol.*, 2021, **181**, 1063–1071.
4. Q. Liu, J. J. Yang, X. G. Luo, Y. F. Miao, Y. Zhang, W. T. Xu, L. J. Yang, Y. X. Liang, W. Weng and M. F. Zhu, Fabrication of a fibrous MnO_2@MXene/CNT electrode for high-performance flexible supercapacitor, *Ceram. Int.*, 2020, **46**, 11874–11881.
5. L. Luo, W. Meng, G. J. Wang, J. Qin, H. Y. He and H. J. Huang, MnO_2 nanoflowers-decorated MXene nanosheets with enhanced supercapacitor performance, *J. Alloy. Compd.*, 2023, **957**, 170411.
6. K. L. Li, P. Zhang, R. A. Soomro and B. Xu, Alkali-induced porous MXene/carbon nanotube-based film electrodes for supercapacitors, *ACS Appl. Nano Mater.*, 2022, **5**, 4180–4186.
7. H. Chen, L. Y. Yu, Z. F. Lin, Q. Z. Zhu, P. Zhang, N. Qiao and B. Xu, Carbon nanotubes enhance flexible MXene films for high-rate supercapacitors, *J. Mater. Sci.*, 2020, **55**, 1148–1156.
8. Y. Yang, X. Y. Huang, C. Y. Sheng, Y. Y. Pan, Y. Huang and X. H. Wang, In-situ formation of MOFs derivatives $CoSe_2$/Ni_3Se_4 nanosheets on MXene nanosheets for hybrid supercapacitor with enhanced electrochemical performance, *J. Alloy. Compd.*, 2022, **920**, 165908.
9. M. Pathak and C. S. Rout, Hierarchical $NiCo_2S_4$ nanostructures anchored on nanocarbons and $Ti_3C_2T_x$ MXene for high-performance flexible solid-state

asymmetric supercapacitors, *Ad. Compos. Hybrid Mater.*, 2022, **5**, 1404–1422.

10. M. Pathak, S. R. Polaki and C. S. Rout, High performance asymmetric supercapacitors based on $Ti_3C_2T_x$ MXene and electrodepositedspinel $NiCo_2S_4$ nanostructures, *RSC Adv.*, 2022, **12**, 10788–10799.
11. W. W. Chen, Y. Peng, Z. H. Qiu, X. Zhang and H. J. Xu, 3D hierarchical $Ti_3C_2T_x$ @NiO-reduced graphene oxide heterostructure hydrogel as free-standing electrodes for high performance supercapacitor, *J. Alloy. Compd.*, 2022, **901**, 163614–163624.
12. Y. C. Wang, Y. Y. Liu, Z. Chen, M. Zhang, B. Y. Liu, Z. H. Xu and K. Yan, In situ growth of hydrophilic nickel-cobalt layered double hydroxides nanosheets on biomass waste-derived porous carbon for high-performance hybrid supercapacitors, *Green Ch. E.*, 2022, **3**, 55–63.
13. T. T. Chen, L. Luo, X. Wu, Y. L. Zhou, W. Yan, M. Z. Fan and W. G. Zhao, Three dimensional hierarchical porous nickel cobalt layered double hydroxides (LDHs) and nitrogen doped activated biocarbon composites for high-performance asymmetric supercapacitor, *J. Alloy. Compd.*, 2021, **859**, 158318–158329.
14. X. M. Guo, H. L. Liu, Y. C. Xue, J. L. Chen, X. H. Wan, J. H. Zhang, Y. J. Liu, A. H. Yuan, Q. H. Kong and H. Fan, NiAl layered double hydroxide flowers with ultrathin structure grown on 3d graphene for high-performance supercapacitors, *Eur. J. Inorg. Chem.*, 2019, **32**, 3719–3723.
15. S. Verma, V. Gupta, A. Khosla, S. Kumar and S. Arya, High performance asymmetric supercapacitor based on vertical nanowire arrays of a novel Ni@Co-Fe LDH core@shell as negative and $Ni(OH)_2$ as positive electrode, *Nanotechnology*, 2020, **31**, 245401–245415.
16. A. Sharifi, M. Arvand and S. Daneshvar, Flexible fiber-shaped supercapacitor based on hierarchically $Co(OH)_2$ nanosheets@NiCo LDH nanoworms/3d-Ni film coated on the binary metal wire substrate for energy storage application, *J. Inorg. Organomet. P.*, 2023, **33**, 761–770.
17. Y. L. Chen, J. Yang, H. Yu, J. Q. Zeng, G. Li, B. B. Chang, C. Wu, X. W. Guo, G. R. Chen, L. P. Zheng and X. Y. Wang, Design and preparation of NiCoMn

ternary layered double hydroxides with a hollow dodecahedral structure for high-performance asymmetric supercapacitors, *ACS Appl. Energy Mater.*, 2022, **5**, 6772–6782.

18. J. Kumar, R. R. Neiber, Z. Abbas, R. A. Soomro, A. BaQais, M. A. Amin and Z. M. El-Bahy, Hierarchical NiMn-LDH hollow spheres as a promising pseudocapacitive electrode for supercapacitor application, *Micromachines*, 2023, **14**, 487–499.
19. L. J. Zhang, X. G. Zhang, L. F. Shen, B. Gao, L. Hao, X. J. Lu, F. Zhang, B. Ding and C. Z. Yuan, Enhanced high-current capacitive behavior of graphene/CoAl-layered double hydroxide composites as electrode material for supercapacitors, *J. Power Sources,* 2012, **199**, 395–401.
20. Y. X. Liu, Y. Z. Wang, C. J. Shi, Y. J. Chen, D. Li, Z. F. He, C. Wang, L. Guo and J. M. Ma, Co-ZIF derived porous NiCo-LDH nanosheets/N doped carbon foam for high-performance supercapacitor, *Carbon*, 2020, **165**, 129–138.
21. M. Li, J. P. Cheng, F. Liu and X. B. Zhang, 3D-architectured nickel-cobalt-manganese layered double hydroxide/reduced graphene oxide composite for high-performance supercapacitor, *Chem. Phys. Lett.*, 2015, **640**, 5–10.
22. Z. L. Zhao, X. M. Wu, C. Y. Luo, Y. Wang and W. X. Chen, Rational design of $Ti_3C_2Cl_2$ MXenes nanodots-interspersed MXene@NiAl-layered double hydroxides for enhanced pseudocapacitor storage, *J. Colloid Interf. Sci.*, 2022, **609**, 393–402.
23. X. M. Wu, B. Huang, Q. G. Wang and Y. Wang, High energy density of two-dimensional MXene/NiCo-LDHs interstratification assembly electrode: Understanding the role of interlayer ions and hydration, *Chem. Eng. J.*, 2020, **380**, 122456–122464.
24. J. Pan, S. B. Li, L. Zhang, F. B. Li, Z. F. Zhang, T. T. Yu and D. Q. Zhang, Designed formation of 2D/2D hierarchical V_2CT_x MXene/NiV layered double hydroxide heterostructure with boosted electrochemical performance for asymmetric supercapacitors, *J. Energy Storage*, 2022, **55**, 105415–105423.
25. R. J. Zhang, J. D. Dong, W. Zhang, L. N. Ma, Z. X. Jiang, J. J. Wang and Y. D.

Huang, Synergistically coupling of 3d FeNi-LDH arrays with $Ti_3C_2T_x$-MXene nanosheets toward superior symmetric supercapacitor, *Nano Energy*, 2022, **91**, 106633–106641.

26. J. Zheng, X. Pan, X. Huang, D. Xiong, Y. Shang, X. Li, N. Wang, W. M. Lau and H. Y. Yang, Integrated $NiCo_2$-LDHs@MXene/rGO aerogel: Componential and structural engineering towards enhanced performance stability of hybrid supercapacitor, *Chem. Eng. J.*, 2020, **396**, 1251–1260.
27. C. X. Lu, A. Li, T. F. Zhai, C. R. Niu, H. P. Duan, L. Guo and W. Zhou, Interface design based on Ti_3C_2 MXene atomic layers of advanced battery-type material for supercapacitors, *Energy Storage Mater.*, 2020, **26**, 472–482.
28. R. Z. Zhao, M. Q. Wang, D. Y. Zhao, H. Li, C. X. Wang and L. W. Yin, Molecular-level heterostructures assembled from titanium carbide MXene and Ni-Co-Al layered double-hydroxide nanosheets for all-solid-state flexible asymmetric high-energy supercapacitors, *ACS Energy Lett.*, 2018, **3**, 132–140.
29. W. D. Wang, D. M. Jiang, X. Chen, K. Xie, Y. H. Jiang and Y. Q. Wang, A sandwich-like nano-micro LDH-MXene-LDH for high-performance supercapacitors, *Appl. Surf. Sci.*, 2020, **515**, 145–153.
30. D. D. Zhang, J. Cao, X. Y. Zhang, N. Insin, R. P. Liu and J. Q. Qin, NiMn layered double hydroxide nanosheets in-situ anchored on $Ti_3C_2T_x$ MXene via chemical bonds for superior supercapacitors, *ACS Appl. Energy Mater.*, 2020, **3**, 5949–5964.
31. D. D. Zhang, J. Cao, X. Y. Zhang, N. Insin, S. M. Wang, Y. S. Zhao and J. Q. Qin, NiMn-layered double hydroxides chemically anchored on Ti_3C_2 MXene for superior lithium ion storage, *ACS Appl. Energy Mater.*, 2020, **3**, 11119–11130.